Bandwidth Investigation on Half-Height Pin in Ridge Gap Waveguide

N.B. When citing this work, cite the original published paper.

(article starts on next page)

Bandwidth Investigation on Half-height Pin in Ridge Gap Waveguide

Fangfang Fan, *Member, IEEE,* Jian Yang, *Senior Member, IEEE,*
Vessen Vassilev, and Ashraf Uz Zaman, *Member, IEEE*

Abstract—Gap waveguide is a promising transmission structure, especially for millimeter wave and terahertz applications. That it does not require conductive connection between the upper and the lower plates makes this technology gain advantages over conventional rectangular waveguides and substrate integrated waveguides (SIW) in millimeter-wave and terahertz regime. Different fabrication methods for gap waveguides should be employed for different frequency bands applied, such as molding, milling, die forming, electrical discharge machining (EDM), microelectromechanical systems (MEMS), 3D printing. Therefore, different pin forms used in gap waveguides are required to match the applied fabrication methods. In this paper, a new pin form, the half-height pin form, in gap waveguides is proposed for reducing the fabrication cost, and its stopband characteristics are investigated and compared to the previous full-height pins in gap waveguides at V band. A device of a double-ridged gap waveguide with two $90°$ bends for verifying the stopband characteristic analysis of the new pin form has been designed and manufactured. The measured data confirms our analysis and simulations.

Index Terms—gap waveguide, half-height pin gap waveguide, stopband bandwidth.

I. INTRODUCTION

DURING the last couple of years, a new transmission structure, the so-called gap waveguide, has been proposed for millimeter wave (mmW) and terahertz applications [1], and a series of components based on this technology, such as power dividers, filters, couplers, and antennas, have been designed and verified experimentally [2]–[9]. The gap waveguides have been realized until now by two parallel metal plates, with periodic metal pins on the lower plate to play the role of Artificial Magnetic Conductor (AMC) and smooth surface on the upper plate. No electromagnetic waves can propagate through this pin structure, except along some guiding configurations, such as ridges in ridged gap waveguides [10], microstrip lines in inverted microstrip line gap waveguides [11] or grooves in groove gap waveguides [12], under the condition that the gap between the top of the
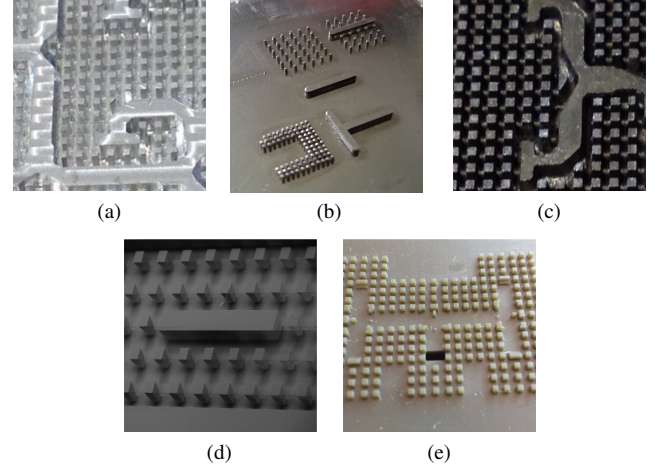

Fig. 1. Different fabrication techniques for gap waveguide technology: (a) Pins and ridges at 60 GHz by milling; (b) Pins and ridges at 60 GHz by die forming; (c) Pins and ridges at 60 GHz by EDM (electrical discharge machining); (d) Pins and ridges at 300 GHz by MEMS (microelectromechanical systems); (e) Plastic pins at 60 GHz by 3D printing, metal surface plating needed.

pins and the upper plate is less than quarter wavelength. Since the waves propagate only along the guiding configurations where the electromagnetic waves are constrained in the air in all types of gap waveguides, there is no dielectric losses, even that dielectric substrates are involved in the structure of inverted microstrip line gap waveguides. Thus, the gap waveguides have the advantage of lower loss compared to microstrip lines and substrate integrated waveguides (SIW), where the waves propagate in dielectric materials.

The fact that it does not require conductive connection between the upper and the lower plates in gap waveguides opens up a lot of possibility and availability for many cost-effective manufacture technologies to be used in mmW and terahertz devices and systems by gap waveguide technology, such as molding, milling, die forming, electrical discharge machining (EDM), microelectromechanical systems (MEMS) and 3D printing. Different fabrication technologies have their own characteristics. Therefore, an optimal fabrication technology should be selected for low-cost manufacture for different pin geometries in gap waveguides. Until now, the existing pin forms are the circular pins [13], the square pins [1], the inverted pyramid-shaped pins [14] and the double cone pins [15]. The first two are the basic forms and the last two are for wideband performance. However, all these pins are quite

Fig. 2. Pin forms for gap waveguide technology: (a) Half-height pin; (b) Full-height pin.

Fig. 3. Analysis model of general pin form for gap waveguide technology: (a) Model for general pins; (b) Equivalent circuit model.

long and thin at mmWs, which poses a difficulty for low-cost manufacture.

The purpose of this paper is to propose and analyze a new pin form: the half-height pins [16], [17] for relaxing the fabrication requirements with the same electrical performance. The paper is organized as follows. In Sect. II we describe characteristics of different fabrication technologies applied to the gap waveguide technology and therefore the motivation of the present work. An analytical model for the new pin structure is set up in Sect. III to describe the basic working principle. Analysis and discussions on the stopband characteristics of the half-height pins with different dimensions are presented in Sect. IV. The misalignment tolerance between the upper pins and the lower pins is analyzed in Sect. V. A device of a double-ridged gap waveguide (DRGW) with two 90° bends for verifying the stopband characteristics of the new pin form is designed and presented in Sect. VI with measurement data. Then, the paper is ended with conclusions.

II. FABRICATION TECHNOLOGIES IN GAP WAVEGUIDE TECHNOLOGY

Different fabrication technologies have their own advantages and disadvantages, and therefore a certain applicability in the gap waveguide technology.

1) Molding is a very cheap fabrication method for mass production. The main drawbacks of this technique for gap waveguide pins are that the pins cannot be thin and long, and the surface is not smooth enough for mmW applications. We have not yet tried this manufacture technique since we are still in the development stage.

2) Milling is an accurate technique for gap pins below 100 GHz. Fig. 1(a) shows a pin structure for a gap waveguide by milling. The main drawbacks of this technique are that the pins cannot be thin and long, and the cost is not low enough for mass production.
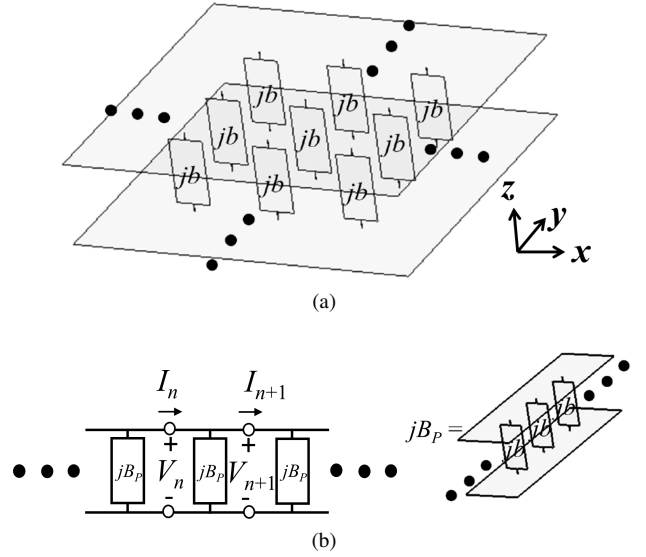
3) Die Forming uses a high pressure on a soft metal material through a die to make pins, as shown in Fig. 1(b), and is a good technique for mass production. The main problem is that it is very difficult to separate the die and the pin plate if the pins are long and thin.

4) EDM is a manufacturing process whereby a desired shape is obtained using electrical discharges, as shown in Fig. 1(c). The main problem is that the pins should not be long and thin, and the die for discharge can be used only for a limited number of times, which makes the mass production cost not very low.

5) MEMS makes dielectric pins by "growing" and then gold surface plating them, which is efficient for gap waveguide pins above 100 GHz for mass production. A pin structure at 300 GHz is shown in Fig. 1(d). However, it is very difficult and expensive for MEMS to make pins at 60 GHz (about 1.25 mm long). If the pin's length at 60 GHz can be short as half (about 0.6 mm long), MEMS becomes attractive for 60-GHz pin structures.

6) 3D printing can only print at the moment plastic pin structure with good tolerance and smooth surface as shown in Fig. 1(e) (direct printing in metal leads to a rough surface which causes a large loss at mmW) and then the 3D plastic pin structure should have metal surface plated, which may cause a rough surface. 3D printing prefers short and thick pins. In addition, 3D printing is not a choice for mass production.

It can be concluded from the above that short and thick pins are much preferred for all manufacture techniques. This is our motivation to propose and analyze the half-height gap waveguide pin form.

III. NEW PIN FORMS AND ANALYSIS MODEL

Fig. 2(a) shows the geometry of the new half-height pin. As a reference, the previous developed square pin form, referred to as the full-height pin in this paper, is presented in Fig. 2(b).
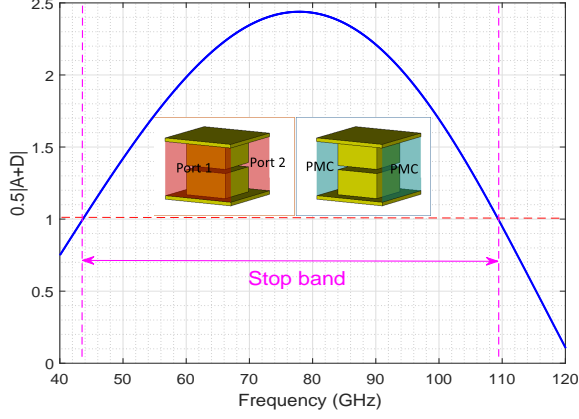
Fig. 4. Simulated result of $|0.5(A + D)|$, where A and D are parameters of the ABCD matrix of the pin equivalent circuit in Fig. 3.
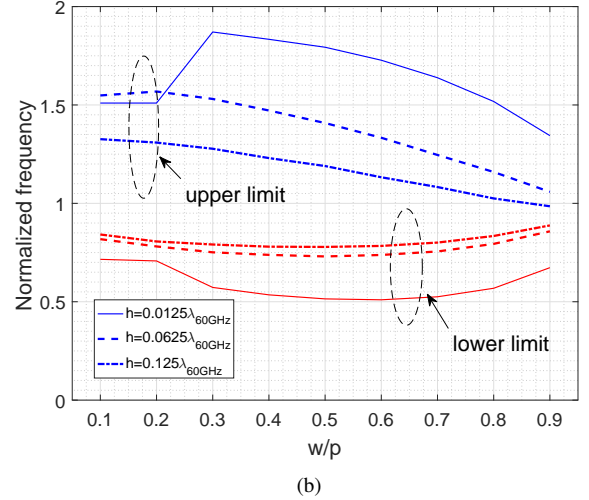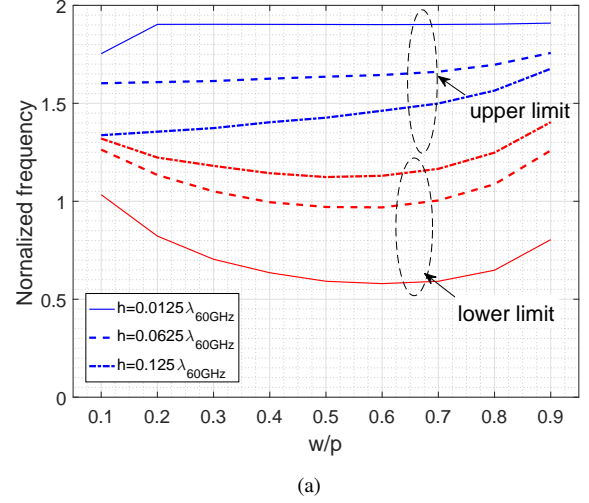

(a)

(b)

Fig. 5. Normalized frequencies over 60 GHz of the stopband with constant values of $p = 0.25\lambda_{60\text{GHz}}$ and $d = 0.25\lambda_{60\text{GHz}}$, and varied values of w and h for half-height pin and full-height pin forms, where $\lambda_{60\text{GHz}} = 5$ mm is the wavelength at 60 GHz: (a) Half-height pin; (b) Full-height pin.

The half-height pin in Fig.2(a) has the air gap between the upper and the lower pin plates. From the simulations shown in the next section, the optimal value of the pin's length is a half of the previous developed pins, which is the reason for its name.

The half-height pin form has a symmetry between the upper and the lower plates. The upper PEC (perfect electric conductor) and the lower PMC (perfect magnetic conductor) model for full-height pin gap waveguides is not valid for the half-height pin structure. An analysis model of a general pin form for gap waveguides is shown in Fig. 3(a): each pin (or each pair of the upper and the lower pins in our case) can be modeled by an admittance jb in a parallel-plate waveguide. All propagating waves are composed by two basic modes: x-direction propagating waves and y-direction propagating waves. A stopband is held when and only when no x-direction waves and no y-direction waves propagate in a certain frequency band. Therefore, we need to analyze only the x-direction waves due to the same configuration and dimensions of the pin geometry in x- and y- directions. The equivalent circuit for x-direction waves is shown in Fig. 3(b), where the admittance of jB_P is composed of a column of infinite parallel admittances of jb separated by a distance p in y-direction. An infinite cascaded two-port network can be used for the analysis of the periodic structure [18], where voltages V_n, V_{n+1} and currents I_n, I_{n+1} on the nth unit cell as shown in Fig. 3(b) are related with a $ABCD$ matrix as:

$$\begin{bmatrix} V_n \\ I_n \end{bmatrix} = \begin{bmatrix} A & B \\ C & D \end{bmatrix} \begin{bmatrix} V_{n+1} \\ I_{n+1} \end{bmatrix}. \tag{1}$$

The equivalent circuit of the pin unit is composed of three two-port networks cascaded one after another: a transmission line of length $(p-w)/2$ representing a piece of parallel waveguide with a characteristic impedance Z_0, a shunt susceptance of b_0 normalized to Z_0, and another transmission line of length $(p-w)/2$. Then, we have the following normalized $ABCD$ matrix:

$$\begin{bmatrix} A & B \\ C & D \end{bmatrix}$$
$$= \begin{bmatrix} \cos\frac{\theta}{2} & j\sin\frac{\theta}{2} \\ j\sin\frac{\theta}{2} & \cos\frac{\theta}{2} \end{bmatrix} \begin{bmatrix} 1 & 0 \\ jb_0 & 1 \end{bmatrix} \begin{bmatrix} \cos\frac{\theta}{2} & j\sin\frac{\theta}{2} \\ j\sin\frac{\theta}{2} & \cos\frac{\theta}{2} \end{bmatrix} \tag{2}$$

where $\theta = k(p - w)$, with the propagation constant k of the parallel-plate waveguide, p the length of the period for unit cell and w the width of the pin. From [18], the requirement for no wave propagation in the pin structure is

$$0.5|A + D| = |\cos\theta - \frac{b_0}{2}\sin\theta| > 1 \tag{3}$$

IV. STOPBAND ANALYSIS FOR HALF-HEIGHT PINS

The CST model is shown in Fig. 4 for analyzing a half-height pin unit with $p = 1.71$ mm, $d = 1.31$ mm, $w = 0.79$
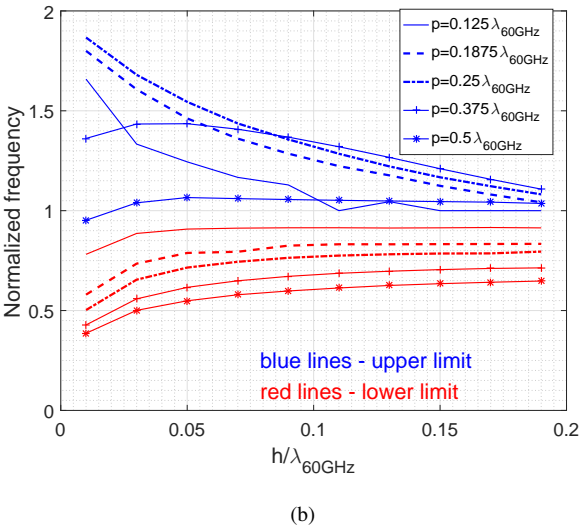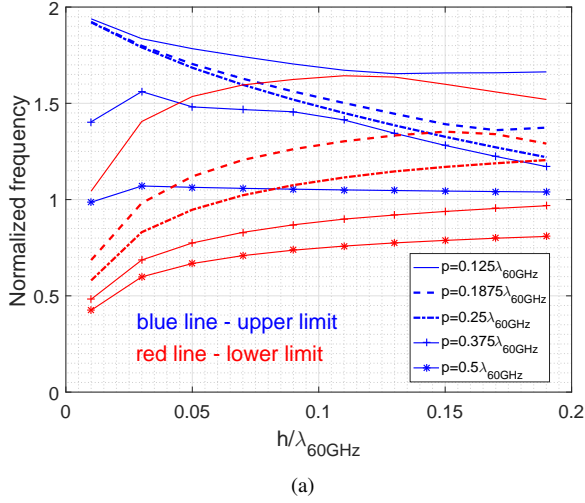
(a)

(b)

Fig. 6. Normalized frequencies over 60 GHz of the stopband with constant $w = 0.1\lambda_{60\text{GHz}}$, $d = 0.25\lambda_{60\text{GHz}}$ and varied p, h for (a) Half-height pin and (b) Full-height pin.
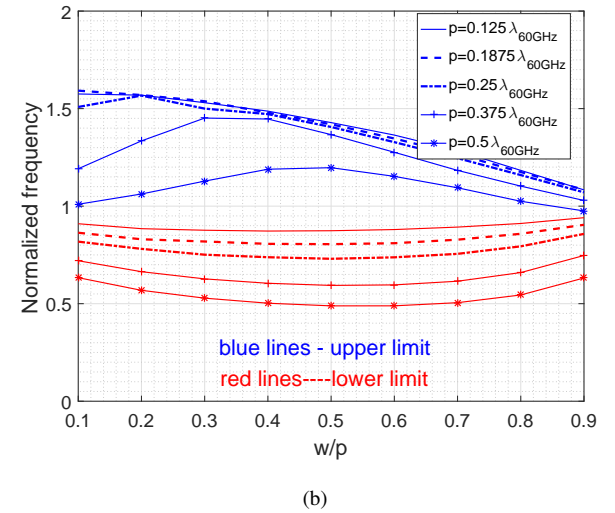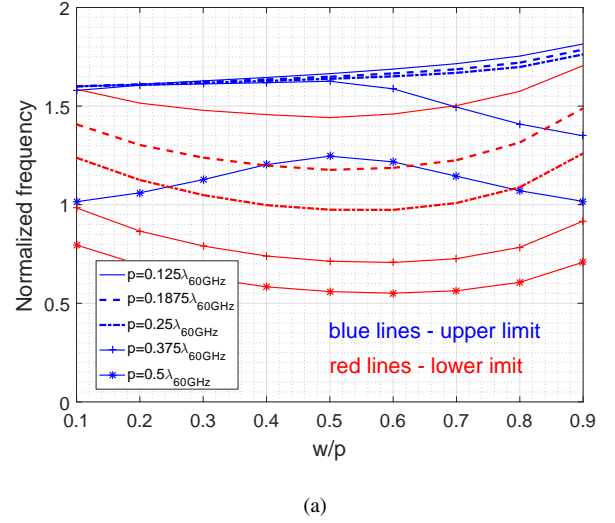

(a)

(b)

Fig. 7. Normalized frequencies over 60 GHz of the stopband with constant $h = 0.0625\lambda_{60\text{GHz}}$, $d = 0.25\lambda_{60\text{GHz}}$ and varied w, p for (a) Half-height pin and (b) Full-height pin.

mm and $h = 0.26$ mm. The two PMC side walls are defined in order to make the periodical structure in y-direction. The $ABCD$ matrix of the unit cell can be extracted from CST simulated data. The simulated value of $0.5|A + D|$ is shown in Fig. 4, indicating that the stopband is from 43.68 GHz to 109.40 GHz (where $0.5|A + D| > 1$). The same structure has been also full-wave analyzed by using the Eigenmode solver in CST, which gives a stopband from 43.28 GHz to 106.52 GHz. Therefore, the model for operation mechanism of the general pin form by using equivalent circuit method has a satisfactory accuracy and can be used to understand the working principle of the half-height pin gap waveguide.

The stopband characteristics of the half-height pin form have been investigated by using both the above mentioned analysis model and numerical software CST Eigenmode solver. We choose the narrower bandwidth from the two methods in order to guarantee the wave stop. The stopband characteristics of half-height pins, both the bandwidth and the center frequency of stopband, are varied with all pin's

parameters: period p, width w, gap height h and length d. Therefore, we choose to present the stopband characteristics with two varied parameters and two fixed parameters with frequencies normalized by 60 GHz in each of figures from 5 to 8.

Fig. 5 shows both the upper $f_{\max}$ and the lower $f_{\min}$ limits of the stopband for both the half-height and the full-height pin forms with fixed values of $p = 0.25\lambda_{60\text{GHz}}$ and $d = 0.25\lambda_{60\text{GHz}}$, and varied values of w and h. Note that $\lambda_{60\text{GHz}}$ is the wavelength at 60 GHz, not the center frequency of the stopband. It can be seen from Fig. 5 that the stop bandwidth for both pin forms is enlarged when h decreases, and the optimal value of w/p for the largest ratio bandwidth $f_{\max} : f_{\min}$ is 0.5–0.7 for the half-height pins and 0.3–0.5 for the full-height pins, respectively. In addition when $w/p = 0.8 - 0.9$ (very thick pins) with $h = 0.0125\lambda_{60\text{GHz}}$, the stop bandwidth is about 2.7:1 for the half-height pins but 2:1 for the full-height pins. This indicates that the half-height pin gap waveguide can have thicker and shorter pins than the full-height pin gap
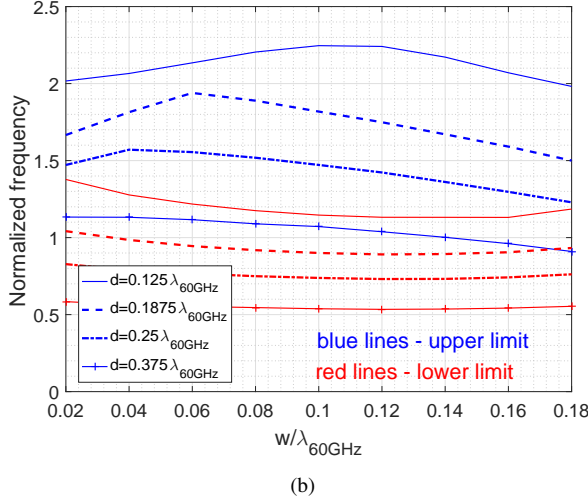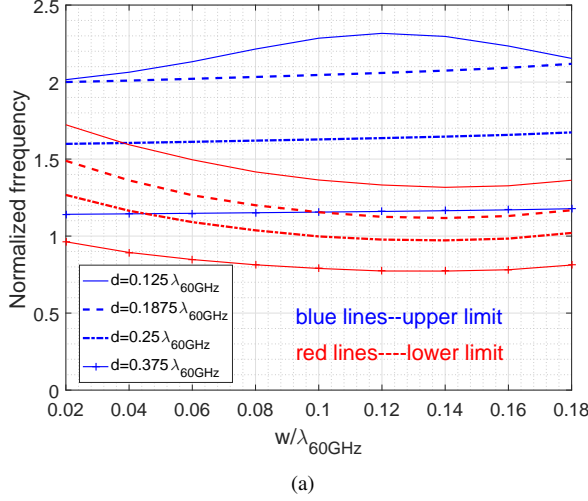
(a)

(b)

Fig. 8. Normalized frequencies over 60 GHz of the stopband with constant $p = 0.25\lambda_{60\text{GHz}}$, $h = 0.0625\lambda_{60\text{GHz}}$ and varied w, d for (a) Half-height pin and (b) Full-height pin.
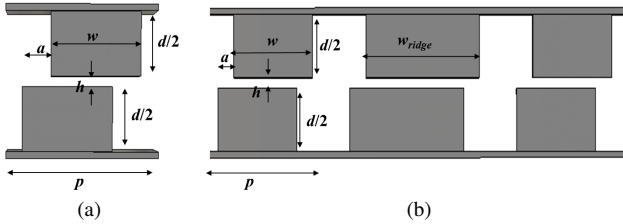

Fig. 9. Definition of offset a in pin unit cell and in double-ridged gap waveguide with half-height pins: (a) Offset of pin cell; (b) Offset of double-ridged gap waveguide.

waveguide.

Fig. 6 is for the case of varied h and p with $d = 0.25\lambda_{60\text{GHz}}$ and $w = 0.1\lambda_{60\text{GHz}}$. From the figure, we can conclude for this case that smaller h makes larger stop bandwidth, and the optimal values of p for the largest stop bandwidth are between $0.25\lambda_{60\text{GHz}}$ and $0.375\lambda_{60\text{GHz}}$, for both the half-height pin and the full-height pin forms.
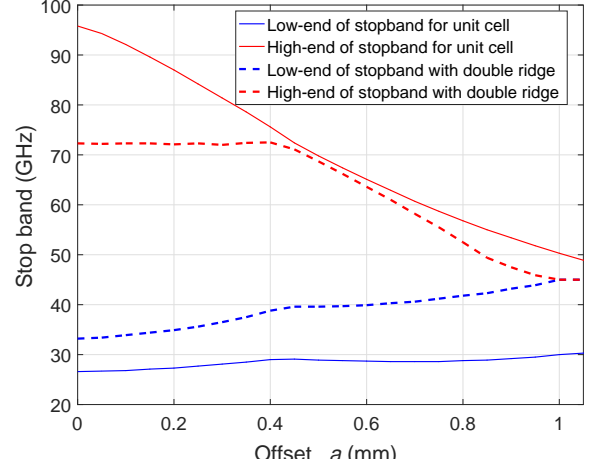

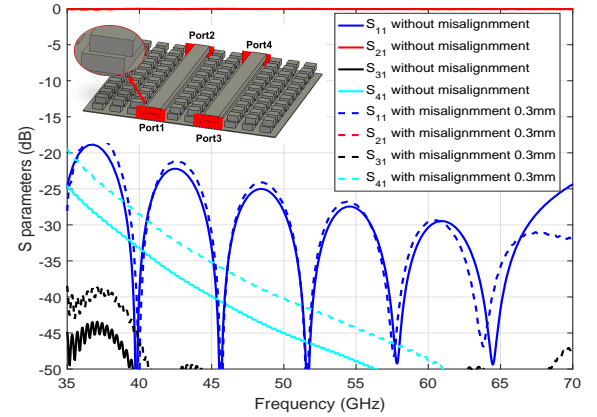Fig. 10. Simulated low end and high end of the stopband with varied offset a.

Fig. 11. S-parameters of a network with two parallel double-ridged transmission lines with and without a misalignment of $a = 0.3$ mm. Note that the upper plate is not shown for clarity of the misalignment between the upper and the lower pins.

The case of varied p and w with $d = 0.25\lambda_{60\text{GHz}}$ and $h = 0.0625\lambda_{60\text{GHz}}$ is shown in Fig. 7. The optimal value of p for the largest stop bandwidth is about $0.375\lambda_{60\text{GHz}}$ for both the half-height and the full-height pins, and the stop bandwidth is about $1.6 : 1$ for the half-height pins and about $1.3 : 1$ for the full-height pins when $w/p = 0.9$.

Fig. 8 shows the results for varied w and d with $p = 0.25\lambda_{60\text{GHz}}$ and $h = 0.0625\lambda_{60\text{GHz}}$. From the figure, it can be seen that with the increase of d, both the upper $f_{\max}$ and the lower $f_{\min}$ limits shift to lower frequencies with almost unchanged stop bandwidth, which is expected. So d has no influence on the bandwidth but determines the center frequency of the stopband.

From all the results shown above, we can conclude: 1) The air gap h is a main factor to define the stop bandwidth. The smaller h, the larger stop bandwidth, for both the half-height pin and the full-height pin forms. 2) Larger pin width does not reduce the stop bandwidth significantly for the half-height
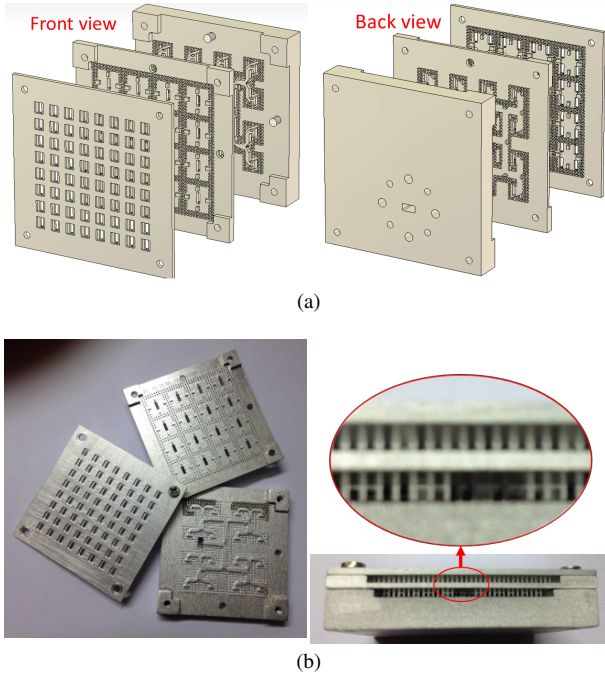
(a)

(b)

Fig. 12. Application example of half height pin gap waveguides: a V-band 8×8 slot array antenna using half height pins for feeding network: (a) Geometry of the antenna; (b) Prototype (left) and a side view (right) through pins to show a good alignment for the whole antenna by checking the alignment of upper and lower pins.

(a)   (b)
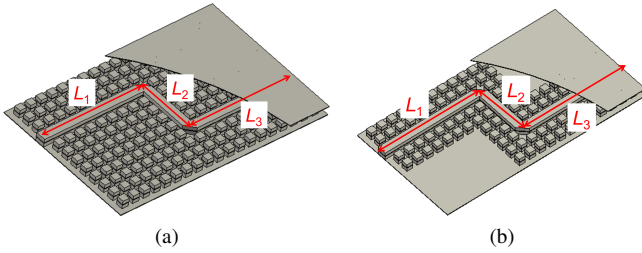
Fig. 13. CST models of the verification devices of two 90° bends: (a) With many rows of pins; (b) With only two rows of pins, where all dimensions are listed in Table I.

pins but does for the full-height pins. 3) Period p has also a significant influence on the stop bandwidth, so p should be between 0.25λ and 0.375λ. 4) The pin length d determines the center frequency of the stopband.

V. TOLERANCE ANALYSIS OF MISALIGNMENT

One natural question arises with the introduction of the half-height pin structure: how does a misalignment between

TABLE I
DIMENSIONS OF DRGW FOR TOLERANCE ANALYSIS.

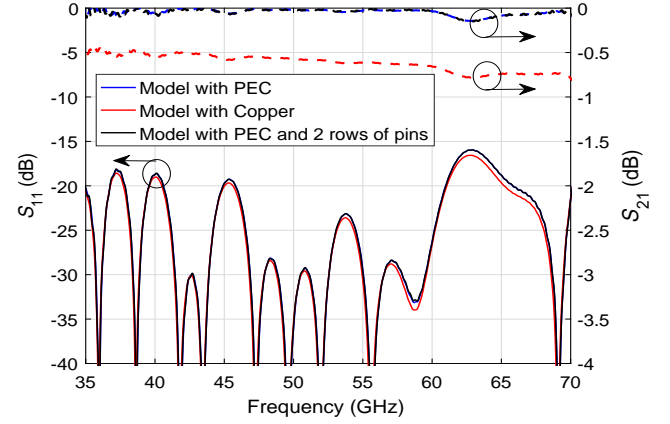| Parameter	Value (mm)	Parameter	Value (mm)
$d/2$	0.7	L_1	20.575
w	1.25	L_2	10.5
h	0.118	L_3	20.375
p	2.1	W_{ridge}	1.8

Fig. 14. Simulated S-parameters of the verification device of two 90° bend double-ridge gap waveguide with half-height pins for 3 cases: modeled by PEC, modeled by a lossy Copper ($\sigma = 5.8 \times 10^7$ S/m) and modeled by PEC with only two rows of pins.
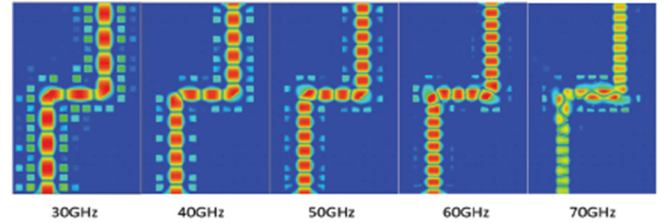

Fig. 15. Simulated field distribution of the verification device of two-90°-bend double-ridge gap waveguide with half-height pins.

the upper and the lower pins affect the performance? A tolerance analysis of this misalignment has been carried out with simulations in CST Microwave Studio.

Fig. 9 shows the models of an offset pin unit cell and an offset DRGW for the stopband analysis in CST. The dimensions of the offset pin cell and the DRGW are illustrated in Fig. 13 and Table I except for offset a which will vary for the analysis. Fig. 10 shows the simulated stopband with different values of offset a for both the offset pin structure and the offset DRGW. It can be seen that the stopband decreases with the increase of offset a and that the stop bandwidth with the DRGW offset or non-offset is smaller than that of only the pin structure offset or non-offset. This is because the definition of the stopband for ridged gap waveguides is the band where all modes are stopped to propagate except for the quasi-TEM mode (the dominate mode in the ridge gap waveguide) along the ridges. Since higher order modes in the DRGW appear before the pin structure propagation modes, the stop bandwidth for DRGW is reduced. For example, with the full offset ($a = 1.05$ mm) where the upper pin are in the middle of the lower pin, there is still a narrow stopband from 30 GHz to 50 GHz for the pin structure. However, when the DRGW is offset with a larger than 1 mm, there is no stopband, which means that higher order DRGW modes can propagate along the ridges at the same time with the quasi-TEM mode. Nevertheless, if offset a is smaller than 0.4 mm for the gap
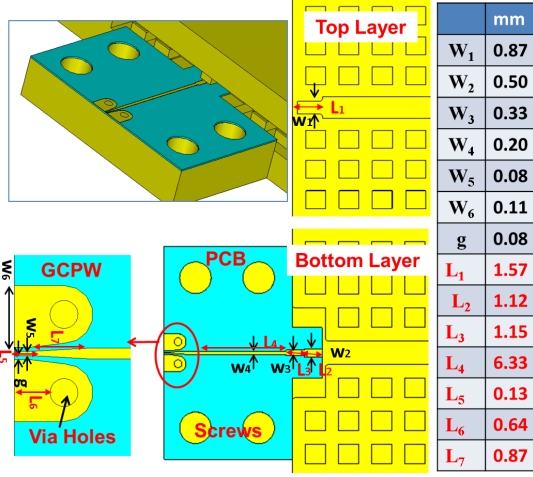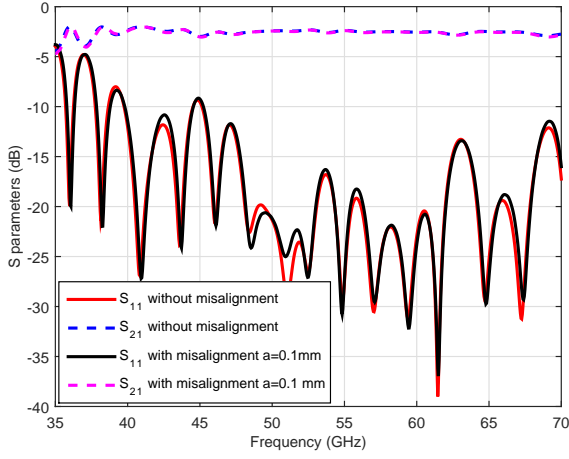
Fig. 16. Geometry of the transition of DRGW-μstripLine-GCPW.

Fig. 17. Simulated S-parameters of the transition of DRGW-μstripLine-GCPW with and without a misalignment of offset $a = 0.1$ mm.
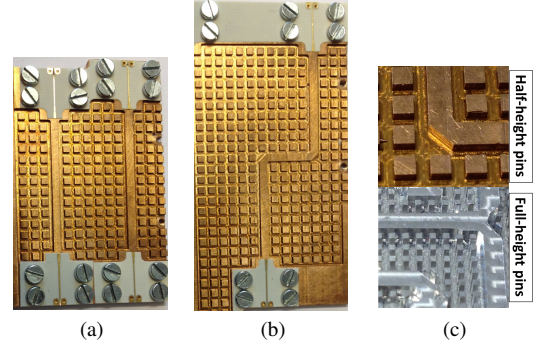

Fig. 18. Manufactured devices: (a) The lower plater of the TRL Cal kit with the THRU and the LINE while the REFLECT is made by inserting a piece of Copper strip between the upper ridge and the lower ridge (not shown here); (b) The lower plate of the verification device with two $90°$ bends; (c) Comparison between the half-height and a previous full-height pins at 60 GHz with the same scaled photo.
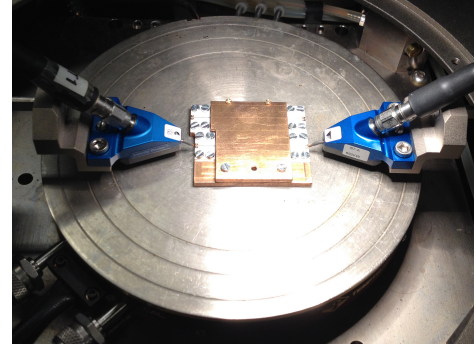

Fig. 19. Setup of the measurement.

waveguide (a very large value for manufacture tolerance), the stopband is kept almost unchanged from 40 GHz to 72 GHz.

Fig. 11 shows another investigation on the offset tolerance: two parallel double-ridged lines are separated by two rows of the half-height pins with or without a misalignment of offset $a = 0.3$ mm between the upper plate and the lower plate (so both the ridges and pins are offset). The figure shows that the S-parameters, both the reflection coefficient S_{11} and the mutual couplings S_{31} and S_{41} among port 1, port 3 and port 4, are almost unchanged with this misalignment. Therefore, we can conclude that if offset a is smaller than 20% of the width of the pins, the performance of the half-height pin gap waveguide is almost not affected by the misalignment offset.

It is worth pointing out that even for full-height pin gap waveguide antennas, the alignment is also very critical since anyway a feeding network should have a good alignment to coupling slots or cavities, etc., in a whole antenna structure. Actually, by using the half-height pin gap waveguide, a good alignment can be easily achieved. Fig. 12 shows a planar

array antenna prototype with half-height pins, where a good alignment was achieved by aligning the upper pins with the lower pins through the side openings, instead of using expensive and difficult positioning posts for alignment. Please refer to [19] for detailed design of the slot array antenna using the half-height pins at V-band.

For the tolerance analysis, the misalignment tolerance is the one only half-height-pin gap waveguides have. The other dimension tolerance requirements, i.e. pin width w, pin length d, gap height h and pin period p, can be indicated from Fig. 5 to Fig. 8 for both the half height pins and the full height pins. For example, from Fig. 5 if we assume a fixed p, the variation of w affects the stop bandwidth in the half-height-pins' case less than in the full-height-pins' case with the optimal values of w/p over 0.5–0.7 for the half height pins and over 0.3–0.5 for the full height pins. Figs. 6–8 show the same conclusion that the half height pins have better tolerance performance due to that the curves for half height pins are flatter than those for the full height pins.

VI. VERIFICATION AND MEASUREMENTS

To verify the transmission characteristic of the gap waveguide using the half-height pin form, a prototype of a DRGW with two $90°$ bends and transitions to microstrip lines at the two ends has been fabricated and measured.
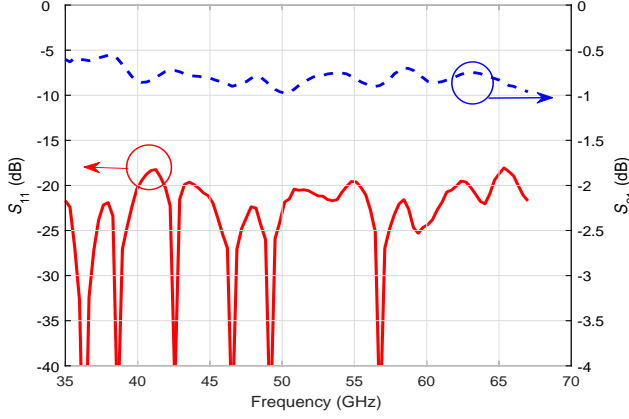
Fig. 20. Measured S-parameters of the verification device of the two-90°-bend double-ridge gap waveguide with half-height pins.

A. Two 90° Bends

The CST model of the verification device with a DRGW employing half-height pins, by PEC, lossy Copper (annealed) ($\sigma = 5.8 \times 10^7$ S/m) and PEC with only two rows of the pins, is shown in Fig. 13. It has two 90° bends. The reason to use the two-90°-bend for the verification is that the bends introduce higher order modes at the positions of the bends, and therefore it is a tougher test than a straight line to see if the half-height pins can stop all propagating modes in the pin structure. The dimensions of the pins, ridge and bends are shown in Table I. The simulated S-parameters are shown in Fig. 14, over the frequency band from 35 GHz to 70 GHz, with S_{11} below -15 dB. It can be seen that the leakage loss is very small (close to 0 dB) based on $S_{11}^2 + S_{21}^2$ for the models by PEC, even with only two rows of the pins (hardly see the difference between the PEC model with many rows and only two rows of the pins), and the ohmic loss due to the lossy Copper is from 0.5 dB to 0.8 dB over the frequency band, a major factor for losses. The field distribution of the two-90°-bend from 30 GHz to 70 GHz is shown in Fig. 15, stating a very good propagation only along the double ridge gap waveguide with only two rows of the pins.

A full analysis of Q factor and losses of half-height-pin double-ridged gap waveguides and groove gap waveguides has been presented in [20], where it is concluded that half-height-pin gap waveguides have the nearly identical Q factors as full-height-pin gap waveguides.

B. Transition from Gap Waveguide to GCPW

We use in this work a wideband (35 GHz to 70 GHz) transition from the DRGW to microstrip line (μstripLine) and then to grounded coplanar waveguide (GCPW) for measuring the verification device with a wafer-probe, instead of using two transitions from DRGW to two standard rectangular waveguides presented in [17]. A similar transition from a microstrip line to a full-height pin ridge gap waveguide was reported in [21]. Fig. 16 shows the diagram of the transition: the PCB of Rogers RO4350B with $\varepsilon_r = 3.66$ and 0.118 mm thick (the

same as the air gap of the DRGW) is inserted into the middle of the double ridge with the top ridge touching the microstrip line. Four screws are used to connect the back bottom via-hole metal layer to get the grounding. The simulated S-parameters of the whole verification device (two-90°-bend DRGW + two DRGW-μstripLine-GCPW transitions) are shown in Fig. 17, with and without a misalignment of $a = 0.1$ mm. It can be seen that S_{11} is a bit high (about -5 dB) at both ends of the frequency band due to such a wide bandwidth for DRGW-μstripLine-GCPW transitions but not very sensitive to the misalignment so we decide to design and manufacture our own TRL calibration kit as shown in Fig. 18 to calibrate out the effects of the transitions and the connection between GSG probe and the GCPW. Note that the figure shows only the THRU and the LINE while the REFLECT is made by inserting a piece of Copper strip between the upper ridge and the lower ridge, which could not be shown in the figure.

C. Measured Results

Fig. 18 shows the TRL cal kit and the verification device, manufactured by a computer numerical control (CNC) milling machine. The PCBs of the transitions were fabricated by standard photolithography process. All strips on the PCB are gold plated to guarantee a good conductive contact with the wafer-probe for the measurement. A comparison of the size between the present half-height pins and the previous full-height pins is also shown in Fig. 18 with the same scaled photos, which tells that the half-height pins can be much shorter and thicker than the full-height pins, providing a possibility for low-cost pin manufacture. The measurement setup is shown in Fig. 19. The measurement result after calibration process by using the TRL calibration kit is shown in Fig. 20. Note that we can only measure up to 67 GHz due to the limitation of our GSG probe. Compared to the red curve for lossy Copper modeling in Fig. 14, the measured reflection coefficient S_{11} agree well with the simulated data, and the insertion loss S_{21} is between 0.3 dB and 0.5 dB lower than the simulated data, which we believe is due to the surface roughness. However, we have no means to measure the surface roughness at the moment so we haven't verified this statement by simulations.

VII. CONCLUSION

A new pin form for the gap waveguide technology, the half-height pins, was proposed and analyzed. From the analysis, simulations and measurements, the half-height pins have just a half length of the full-height pins, and can have a wider pin width than the full-height pins, with a similar electrical performance on stopband. The tolerance for the misalignment between the upper and the lower pins should be smaller than 20% of the width of the pins. A verification device, the two-90°-bend with the transitions of DRGW-μstripLine-GCPW was designed, fabricated and measured. The measured data agreed well with the simulated one. The half-height pin gap waveguide provides a possibility to have a low cost for mass production by different manufacture technology.

ACKNOWLEDGMENT

REFERENCES

[1] P.-S. Kildal, E. Alfonso, A. Valero-Nogueira, and E. Rajo-Iglesias, "Local metamaterial-based waveguides in gaps between parallel metal plates," *IEEE Antennas Wireless Propag. Lett.*, vol. 8, pp. 84–87, 2009.

[2] M. S. Sorkherizi, A. Khaleghi, and P.-S. Kildal, "Direct-coupled cavity filter in ridge gap waveguide," *IEEE Trans. Compon. Packag. Manuf. Technol.*, vol. 4, no. 3, pp. 490–495, 2014.

[3] E. A. Alos, A. U. Zaman, and P. Kildal, "Ka-band gap waveguide coupled-resonator filter for radio link diplexer application," *IEEE Trans. Compon. Packag. Manuf. Technol.*, vol. 3, no. 5, pp. 870–879, 2013.

[4] A. U. Zaman, P.-S. Kildal, A. Kishk *et al.*, "Narrow-band microwave filter using high-Q groove gap waveguide resonators with manufacturing flexibility and no sidewalls," *IEEE Trans. Compon. Packag. Manuf. Technol.*, vol. 2, no. 11, pp. 1882–1889, 2012.

[5] A. Berenguer, M. Baquero-Escudero, D. Sanchez-Escuderos, B. Bernardo-Clemente, and V. E. Boria-Esbert, "Low insertion loss 61 GHz narrow-band filter implemented with groove gap waveguides," in *Proc. 44th Europ. Microwave Conf. (EuMC)*, Rome, 2014, pp. 191–194.

[6] A. del Olmo-Olmeda, M. Baquero-Escudero, V. E. Boria-Esbert, A. Valero-Nogueira, and A. J. Berenguer-Verdu, "A novel band-pass filter topology for millimeter-wave applications based on the groove gap waveguide," in *2013 IEEE MTTS Int. Microw. Symp. Dig. (IMS)*, 2013, pp. 1–4.

[7] H. Raza, J. Yang, P.-S. Kildal, and E. Alfonso Alos, "Microstrip-ridge gap waveguide–study of losses, bends, and transition to WR-15," *IEEE Trans. Microw. Theory Techn.*, vol. 62, no. 9, pp. 1943–1952, 2014.

[8] H. Raza and J. Yang, "Compact UWB power divider packaged by using gap-waveguide technology," in *Proc. 6th Europ. Conf. Antennas Propag. (EuCAP)*, Prague, 2012, pp. 2938–2942.

[9] J. Yang and H. Raza, "Empirical formulas for designing gap-waveguide hybrid ring coupler," *Microw. Opt. Technol. Lett.*, vol. 55, no. 8, pp. 1917–1920, 2013.

[10] P.-S. Kildal, A. U. Zaman, E. Rajo-Iglesias, E. Alfonso, and A. Valero-Nogueira, "Design and experimental verification of ridge gap waveguide in bed of nails for parallel-plate mode suppression," *IET Microw. Antennas Propag.*, vol. 5, no. 3, pp. 262–270, 2011.

[11] E. Pucci, A. U. Zaman, E. Rajo-Iglesias, and P.-S. Kildal, "New low loss inverted microstrip line using gap waveguide technology for slot antenna applications," in *Proc. 5th Europ. Conf. Antennas Propag. (EuCAP)*, Rome, 2011, pp. 979–982.

[12] E. Rajo-Iglesias and P.-S. Kildal, "Groove gap waveguide: A rectangular waveguide between contactless metal plates enabled by parallel-plate cut-off," in *Proc. 4th Europ. Conf. Antennas Propag. (EuCAP)*, Barcelona, 2010, pp. 1–4.

[13] ——, "Numerical studies of bandwidth of parallel-plate cut-off realised by a bed of nails, corrugations and mushroom-type electromagnetic bandgap for use in gap waveguides," *IET Microw. Antennas Propag.*, vol. 5, no. 3, pp. 282–289, 2011.

[14] A. U. Zaman, V. Vassilev, P.-S. Kildal, and A. Kishk, "Increasing parallel plate stop-band in gap waveguides using inverted pyramid-shaped nails for slot array application above 60GHz," in *Proc. 5th Europ. Conf. Antennas Propag. (EuCAP)*, Rome, 2011, pp. 2254–2257.

[15] S. Shams and A. Kishk, "Double cone ultra wide band unit cell in ridge gap waveguides," in *Proc. 2014 IEEE Antennas Propag. Soc. Int. Symp. (AP-S)*, 2014, pp. 1768–1769.

[16] J. Yang and F. Fan, "Waveguides and transmission lines in gaps between parallel conducting surfaces (half-height pins and double period pins in both surfaces)," Europ. Patent Appl. EP-15186666.2, Gapwaves AB Sweden, 24 Sept. 2015.

[17] F. Fan, J. Yang, and P.-S. Kildal, "Half-height pins – a new pin form in gap waveguide for easy manufacturing," in *Proc. 10th Europ. Conf. Antennas Propag. (EuCAP)*, Davos, 2016, pp. 1–4.

[18] D. M. Pozar, *Microwave engineering*. John Wiley & Sons, 2009.

[19] P. Taghikhani, J. Yang, and A. Vosoogh, "High gain V-band planar array antenna using half-height pin gap waveguide," in *Proc. 11th Europ. Conf. Antennas Propag. (EuCAP)*, Paris, 2017, pp. 2758–2761.

[20] J. Yang, F. Fan, P. Taghikhani, and A. Vosoogh, "Half-height-pin gap waveguide technology and its applications in high gain planar array antennas at millimeter wave frequency," *accepted by IEICE Trans. Comm.*, June 2017.

[21] A. U. Zaman, T. Vukusic, M. Alexanderson, and P.-S. Kildal, "Design of a simple transition from microstrip to ridge gap waveguide suited for MMIC and antenna integration," *IEEE Antennas Wireless Propag. Lett.*, vol. 12, pp. 1558–1561, 2013.

Fangfang Fan received the B.S. in electromagnetic field and microwave technology from Xidian University, Xian, China, in 2003, and the M.S. degree with the same major from University of Electronic Science and Technology of China, Chengdu, China, in 2006. In 2006, she joined the Science and Technology on Antenna and Microwave Laboratory in Xidian University as an assistant, where she was involved with designing ultra-wideband antennas, microstrip antennas applied in SATCOM and passive circuits. In 2011, she got Ph.D. degree and then was promoted as associated professor. During 2015 to 2016, she was with Chalmers University of Technology as a visiting researcher, and did the research about gap waveguide. She holds 8 granted patents and has authored or coauthored over 20 referred journal and conference papers. Her current research interests involve microwave and millimeter-wave gap waveguide technology, including antenna arrays, filters, couplers, SIW antenna and circuits, planar antennas and reflector and antenna array design in SATCOM. Dr. Fan has served as the reviewer for IEEE AWPL and Progress In Electromagnetics Research.
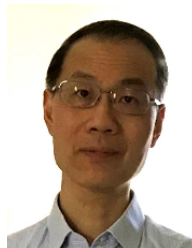
Jian Yang received the B.Sc. degree in electrical engineering from the Nanjing University of Science and Technology, Nanjing, China, in 1982, the M.Sc. degree in electrical engineering from the Nanjing Research Center of Electronic Engineering, Nanjing, in 1985, and the Swedish Licentiate and Ph.D. degrees from Chalmers University of Technology, Gothenberg, Sweden, in 1998 and 2001, respectively. From 1985 to 1996, he was with the Nanjing Research Institute of Electronics Technology, Nanjing, China, as a Senior Engineer. From 1999 to 2005, he was with the Department of Electromagnetics, Chalmers University of Technology, Gothenberg, Sweden, as a Research Engineer. During 2005 and 2006, he was with COMHAT AB as a Senior Engineer. From 2006 to 2010, he was an Assistant Professor, from 2010 to 2016, he was an Associate Professor, and since 2016 he has been a professor with the Department of Signals and Systems, Chalmers University of Technology. His research interests include 60-140GHz antennas, terahertz antennas, MIMO antennas, ultrawideband (UWB) antennas and UWB feeds for reflector antennas, UWB radar systems,UWB antennas in near-field sensing applications, hat-fed antennas, reflector antennas, radome design, and computational electromagnetics.

Vessen Vassilev received the M.Sc. degree in radio communications from the Sofia Technical University, Sofia, Bulgaria, in 1995, and the M.Sc. degree in digital communications and Ph.D. degree from Chalmers University of Technology, Gothenberg, Sweden, in 1998 and 2003, respectively. Between 1998 and 2008, he was working with the development of millimeterwave receivers for applications in radio astronomy and space sciences. Instruments designed by him are currently in operation at the Atacama Pathfinder Experiment (APEX) telescope and at the Onsala Space Observatory. Since 2008, he has been with the Microwave Electronics Laboratory, Department of Microtechnology and Nanoscience, Chalmers University of Technology, Gothenberg, Sweden. His current interests are in the development mm-wavelength sensors based on monolithic microwave microwave integrated circuit technologies.

Ashraf Uz Zaman was born in Chittagong, Bangladesh. He received his BSc. in Electrical and Electronics Engineering from Chittagong University of Engineering and Technology, Bangladesh. He received his MSc. and PhD degree from Chalmers University of Technology, Sweden in 2007 and 2013 respectively. At present, he is an assistant professor with the Communication and Antenna System (CAS) division in the department of Electrical Engineering of the same university. His main research interest includes millimeter and sub millimeter waveguide technology, frequency selective surfaces, microwave passive components, packaging techniques, integration of MMIC with the antennas, active antenna and high efficiency slot array antennas etc.